

Convective activity in the Labrador Sea: Preconditioning associated with decadal variability in subsurface ocean stratification

Ken-ichi Mizoguchi,¹ Steven L. Morey,² Jorge Zavala-Hidalgo,² Nobuo Suginoara,³ Sirpa Häkkinen,⁴ and James J. O'Brien²

Received 3 December 2002; revised 25 April 2003; accepted 4 August 2003; published 21 October 2003.

[1] The decadal variability of the convective activity in the Labrador Sea is investigated using 43 years of model output from a prognostic coupled ice-ocean model that simulates both the Arctic and the North Atlantic Oceans. The fields of the surface density and the mixed-layer depth indicate that the center of the convective activity is located in western Labrador Sea. The decadal variations of the convective depth are controlled to large extent by the oceanic preconditioning associated with changes in subsurface stratification. The intensity of the convective mixing varies from year to year, depending upon how strong the isopycnal doming is at the preconditioning stage at the center of the convective region. The variations of the subsurface stratification seem to be related to the subsurface temperature changes. **INDEX TERMS:** 1620 Global Change: Climate dynamics (3309); 4215 Oceanography: General: Climate and interannual variability (3309); 4255 Oceanography: General: Numerical modeling; **KEYWORDS:** decadal oscillation, North Atlantic, convection, Labrador Sea

Citation: Mizoguchi, K., S. L. Morey, J. Zavala-Hidalgo, N. Suginoara, S. Häkkinen, and J. J. O'Brien, Convective activity in the Labrador Sea: Preconditioning associated with decadal variability in subsurface ocean stratification, *J. Geophys. Res.*, 108(C10), 3330, doi:10.1029/2002JC001735, 2003.

1. Introduction

[2] The Labrador Sea (LS) is a particularly interesting region of the ocean from a dynamic perspective. Here the deep water communicates with the sea surface via convection, which can significantly modify the meridional overturning circulation at the decadal timescales [Holland *et al.*, 2001]. Therefore the variations of the convective activity in the LS at the decadal timescales are expected to be closely linked to decadal variations in the North Atlantic. Deser and Blackmon [1993] showed that a 12- to 14-year decadal oscillation exists in the North Atlantic using the empirical orthogonal function (EOF) analysis technique applied to the sea surface temperature anomaly (SSTA) field. They also suggested a close link between the basin wide decadal oscillation and the variation of the ice concentration in the LS. Mizoguchi *et al.* [1999] demonstrated that alternating warm and cold SSTA propagate from the LS eastward with an approximate 14-year periodicity, using a propagating complex EOF analysis technique.

[3] The strong correlation between the SSTA and sea surface salinity anomalies (SSSA) inside the LS has been recognized in previous studies [Drinkwater, 1994; Reverdin *et al.*, 1997], and the variations of the SSSA are highlighted by the appearance of the Great Salinity Anomalies in the LS in the 1970s (GSA70s) and 1980s (GSA80s) [Dickson *et al.*, 1988; Belkin *et al.*, 1998]. During those years, extremely cold and fresh water anomalies occupied the surface layer and must have had a great impact on the intensity of convection. The decadal periodicity of the GSAs was first postulated by Belkin *et al.* [1998], who analyzed the GSA70s, documented the newly found GSA, and presented evidence of the GSA in the 1990s. The above anomalies peaked in the LS around 1971–1972, 1983–1984, and 1992–1994, respectively, implying a 10- to 11-year period [Reverdin *et al.*, 1997].

[4] Data from Curry *et al.* [1998] showed that there is low frequency variability in the Labrador Sea Water (LSW) thickness. It is directly translated to the intensity of the deep convection, with strong convection producing a thick layer and weak convection associated with relatively thin layer. According to the LSW thickness, the strong convection events occurred roughly in the early 1950s, 1960s, 1970s, and 1990s, indicative of a decadal oscillation. The strong correlation between the ocean surface and the subsurface seems to be closely associated with the decadal variability of the convective activity in the LS. Before discussing the dynamical process in convection at the decadal timescales, perhaps it is necessary to understand how it occurs at very short timescales as compared to decadal timescales, because the physical interpretation at the shorter timescales can

¹GEST, University of Maryland at Baltimore County, Baltimore, Maryland, USA.

²Center for Ocean-Atmospheric Prediction Studies (COAPS), Florida State University, Tallahassee, Florida, USA.

³Frontier Observational Research System for Global Change, Yokohama, Japan.

⁴NASA Goddard Space Flight Center, Greenbelt, Maryland, USA.

directly be applied to that at much longer timescales, as will be shown later on.

[5] One of the prominent features of convection is that it occurs in very localized regions of the northern North Atlantic. Observations [Marshall and Schott, 1999] suggested that there are certain conditions and specific locations that are common to deep-water formation. The surface water needs to be exposed to cold and dry strong winter winds to make it heavy enough to sink to greater depth. In this sense, the open ocean adjacent to boundaries is favored, at which the preferred atmospheric conditions are always supplied from the land or ice surfaces. The weakly stratified water beneath the seasonal thermocline must be brought up to the surface, immediately after the thermocline is eroded due to the surface mixing and cooling. The doming effect of the isopycnals, situated at the center of the cyclonic circulation in the LS, sets up the condition for the weakly stratified water from below to ventilate at the surface [LabSeaGroup, 1998].

[6] As discussed by Killworth [1976], there are basically three different phases in the convective processes. The first is preconditioning, which is followed by the second phase of violent mixing associated with surface cooling, during which vertically homogenized convective chimneys are established. Lastly, the sinking and spreading phase takes place. In the oceanic precondition, there are also three different spatial scales, i.e., plume [Send and Marshall, 1995], eddy [Visbeck et al., 1996] and gyre scales. The first two are non-hydrostatic and have spatial scales of 100 m to 1 km and 5 km to 100 km, respectively. Baroclinic instability plays a major role at these scales. The gyre scale (50–1000 km) determines the large-scale factors that are subject to general circulation and vertical stratification patterns.

[7] Observations have shown that the spatial scale of a convective chimney in the LS is roughly $O(100 \text{ km})$ [Gascard and Clarke, 1983] whereas that of atmospheric buoyancy forcing is $O(500 \text{ km})$. This implies that the gyre-scale oceanic structure has something to do with the selection of a convection site, as well as the intensity of the penetration depth. The convective intensity may be already predetermined by the oceanic preconditioned state, or determined by the combination of both the ongoing buoyancy forcing and the oceanic background stratification before it.

[8] Straneo and Kawase [1999] compared the contribution to a subsequent convective event of localized buoyancy forcing and localized domed isopycnals in the preconditioned ocean. They showed the importance of both the buoyancy forcing and the oceanic preconditioning. Alverson [1995, chapter 4] used a simple one-dimensional mixed-layer model, with an exponentially increasing vertical density profile representing the domed isopycnals and a constant buoyancy forcing, to examine the doming effect of the oceanic background stratification on the intensity of convection. The results showed that with a constant buoyancy input stratification with more sharply domed isopycnals produces a deeper convective mixing.

[9] In this study, the investigation focuses mainly on large-scale convective phenomena related to the oceanic preconditioning in the LS using output from a coupled ice-ocean model. Attention is paid to the dynamical explanation of the convective activity. The model-produced

variability of the mixed-layer depth is approximated by variability associated with the local buoyancy and subsurface stratification in the preconditioned ocean. It is further demonstrated that the decadal variability of the convective depth is strongly correlated to that of the subsurface ocean stratification. The decadal variation of the model may correspond to one of the natural modes of the decadal variability in the ocean.

[10] The model description and data are described in section 2, the results are shown in the context of other observations and compared to an analytical mixed-layer model in section 3. A summary and discussion follow in section 4.

2. Model Description and Data

2.1. Model Description

[11] The coupled ice-ocean model is hydrostatic, Boussinesq and uses the sigma-coordinate system as described by Blumberg and Mellor [1987]. The level 2.5 turbulence closure scheme of Mellor and Yamada [1982] is used to determine the vertical mixing coefficients for momentum and scalar variables. When the stratification is unstable it simply makes the vertical diffusivities large to remove the unstable stratification. For the heat exchange, the bulk formulation is adopted where the heat fluxes are a function of the oceanic surface quantities. The heat exchange with a drag coefficient of 1.3×10^{-3} is used regardless of air-ocean stability conditions [Häkkinen, 1999]. The surface humidity is computed from model generated surface temperature with 95% saturation. The model sea surface temperature (SST) is also used to calculate the upward long-wave radiation. The variability of the salinity in this model is calculated solely by dynamical processes such as advection, mixing and sea ice import. The dynamic-thermodynamic ice model is coupled to the ocean model via interfacial stresses and via salinity and heat fluxes through the ice-water interface. The ice model uses a generalized viscous rheology, as discussed by Häkkinen and Mellor [1992]. The model extends from the Bering Strait to 15°S with resolution of $7/10^\circ$ in longitude by $9/10^\circ$ in latitude in a rotated curvilinear coordinate system. There are a total of 20 sigma-levels in the vertical with higher resolution near the surface. The transports at oceanic lateral boundaries are specified to be 0.8 Sv through the Bering Strait, and 0.8 Sv out at 15°S . At the southern boundary the salinities and temperature are relaxed to Levitus values in five grid rows from the boundary. Restoring of temperature and salinity is also used at the Mediterranean outflow point. This model is forced with modern atmospheric data in order to make the model fields as realistic as possible with an emphasis on the high-latitude simulation due to the ice dynamics. The model is forced with atmospheric climatological data for the first 10 years, after which the COADS anomalies are added to the atmospheric climatologies. The model is run from 1951 to 1993. Only the cloudiness field, the precipitation minus evaporation ($P - E$) field, and the river runoff continue to be climatological. Year-to-year ($P - E$) variations are not important for the formation of the decadal freshwater anomalies as concluded by Houghton and Visbeck [2002] in their study of propagation of the Labrador Sea salinity anomalies. The cloudiness information is given by Interna-

tional Satellite Cloud Climatology Project (ISCCP) measurements. The $(P - E)$ field is obtained from National Centers for Environmental Prediction (NCEP) operational analysis [Rasmusson and Mo, 1996] averaged for 5 years. River runoff, a combination of sources given by Mauritzen and Häkkinen [1997] with an annual total of 18,000 km³, is included, and modifications were added to the $(P - E)$ field at 8°N–12°N to conserve salt in the basin. For a detailed description of the model, readers are referred to Häkkinen [1999].

[12] The coupled ice-ocean model is hydrostatic, and it does not resolve the plume and eddy scales that are mentioned above. Even though the model does not resolve the actual plumes and eddies, water mass formation takes place through vertical diffusion which is determined prognostically using a turbulence closure scheme by Mellor and Yamada [1982]. The assumption of hydrostatic balance is valid when the vertical mixing process is properly parameterized. In this model, enhanced vertical diffusion with an arbitrarily chosen value of vertical diffusivity is used to parameterize convection because the hydrostatic model cannot overturn. Klinger *et al.* [1996, Appendix] showed that vertical diffusion is formally the same as “adjustment” with a finite adjustment timescale.

2.2. Model Output

[13] A 43-year subset of monthly model output from the coupled ice-ocean model covering the LS from 1951 through 1993 is examined. The domain of study extends from 45°N to 65°N, 60°W to 40°W. The density is calculated from the temperature and the salinity using the International Equation of State of Sea Water [United Nations Educational, Scientific and Cultural Organization, 1981]. The forcing fields from the COADS data sets have inherent uncertainties due to historical changes in instrumentation, observation techniques, coding methods, data density, and ship tracking. The data period for the analysis is after the large shift observed by Deser and Blackmon [1993]. All the parameters on the sigma coordinate in the model are linearly interpolated to the 33 level standard depths from the surface to the 5500 m.

3. Results

[14] The objective of this paper is to describe the decadal variability of the deep-water formation in the LS, using the model output obtained from the coupled ice-ocean model, specifically in the region where the deepest convection takes place. For this purpose, a subset of the model domain extending from 45°N to 65°N and 60°W to 40°W is defined. The main focus is to investigate the variability of the temperature, density, and mixed-layer depth (MLD) in the LS and show how strongly oceanic subsurface stratification governs the convection depth, using a simple one-dimensional model.

3.1. Surface and Subsurface Variability

[15] The thickness of the Labrador Sea Water (LSW) layer measured in its formation area was directly related to the intensity of wintertime convection or the MLD in March [Curry *et al.*, 1998, Figure 1c]. Strong convection created a thick layer and weak convection resulted in a

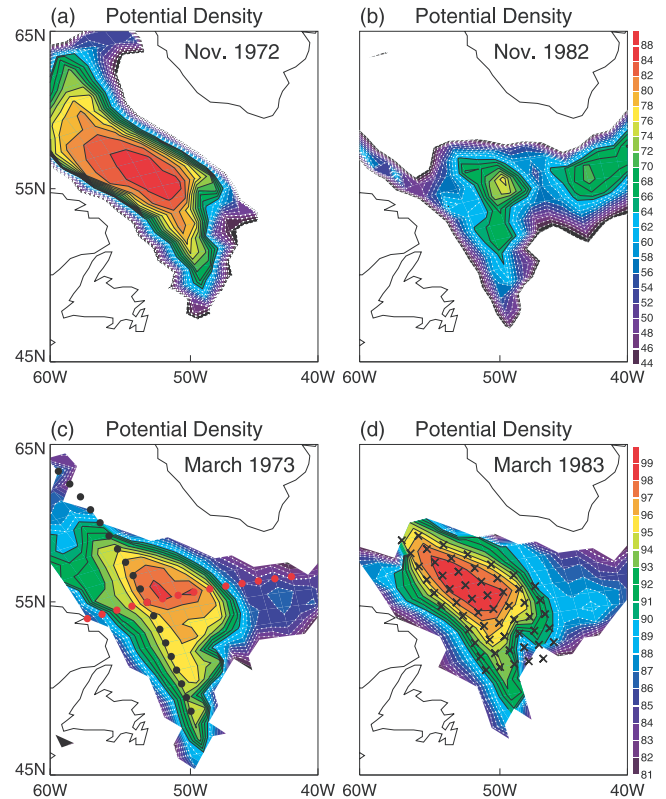


Figure 1. Potential density ($(\sigma_\theta - 27.00) (\text{kg/m}^3) \times 100$) fields at the surface obtained from the coupled ice-ocean model in (a) November 1972, (b) November 1982, (c) March 1973, and (d) March 1983. Only the values above 43 for Figures 1a and 1b, and above 80 for Figures 1c and 1d, are contoured to highlight the region of deep-water formation. The vertical cross-sections shown in subsequent figures are chosen along lines marked by black and red circles in Figure 1c. The cross-hatched region in Figure 1d is considered as the center of convective activity.

relatively thin layer. The time series of LSW thickness showed a clearly sinusoidal decadal behavior with approximately a 10-year period and, according to the observation, strong convection occurred during the early 1960s, 1970s, and 1990s. Analysis of the 1963–1973 OWS Bravo data by Lazier [1980] illustrated that the convection was strongest in 1972 reaching a depth of 1500 m during these years, as was also recognized by Dickson *et al.* [1996]. In contrast to the time series shown by Curry *et al.* [1998], the convection during the 1980s was reported as an apparent deep convection by Dickson *et al.* [2002]. They showed the vertical salinity profiles in the central Labrador Sea since 1950 [Dickson *et al.*, 2002, Figure 1a], in which the deep-mixing event in the 1980s was clearly evident, indicating a homogeneous water column from the surface to a depth of at least 1600 m.

[16] On the basis of the observational evidence, the surface density fields obtained from the coupled ice-ocean model in March 1973 and 1983 (Figures 1c and 1d) are presented here as the typical strong convection events and used to define the convection site. The high surface density in March and the deepest mixed-layer are located in the interior on the western part of the LS basin. Since the LS

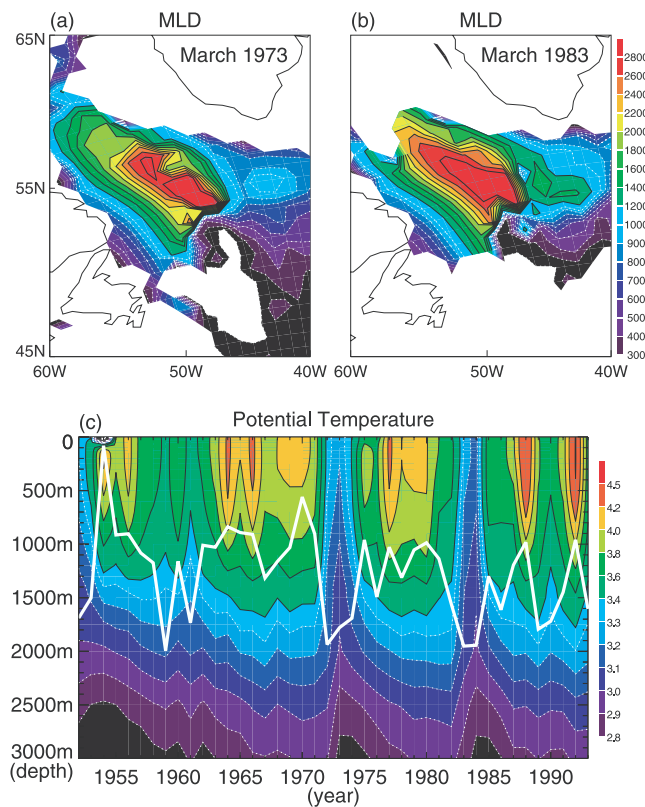


Figure 2. Mixed-layer depth (MLD) obtained from the coupled ice-ocean model in (a) March 1973 and (b) March 1983. The MLD is defined as the depth at which the vertical density difference is less than or equal to 0.005 kg/m^3 . The depth greater than 200 m is contoured. (c) Depth versus time diagram of the model potential temperature in March from 1951 through 1993 averaged over the region shown in Figure 1d. The temperature varies from 1.9°C to 4.4°C . Superimposed is the time series (white line) of the MLD in March obtained from the model. The time series is averaged over the region shown in Figure 1d.

water is weakly stratified, instead of the real value of the potential density (σ_θ), $(\sigma_\theta - 27.00) \times 100$ is shown to present the density fields. The region of deep-water formation, which is represented by 56 data points, is shown in Figure 1d and averaged to obtain a one-point value to specify the possible convection periods and locations. This region covers the active part of the convection that takes place in March 1973 and most of the convection sites are located around this fixed area.

[17] The surface density of the model during the preceding November months (Figures 1a and 1b) shows that there is no correlation between the surface density prior to convection and the strength of convection. That is, prior to the winter of 1973, large values of surface density were evident in the LS; however, this was not the case prior to the winter of 1983. The years 1973 and 1983 were the two strongest convection years of this record. The surface density therefore does not seem to control the subsequent convective activity.

[18] The vertical density difference of 0.005 kg/m^3 between the surface and the mixed-layer base is used to

define the MLD (Figures 2a and 2b). The maximum MLD in the LS in March indicates the deepest convection depth and it corresponds to the largest values of the surface density.

[19] The MLD time series (white line in Figure 2c) is suggestive of decadal variability of the convective activity in the LS. There is a deep-mixing event in the mid 1980s just as strong as the deep ones in the early 1960s, early 1970s and early 1990s, according to the coupled ice-ocean model. During the weak convection years the mixing reaches a depth of approximately 1000 m. The time series fluctuates with an amplitude of over 400 m which is slightly reduced due to the spatial average over the region of deep-water formation. There are three weak and three strong events seen over the course of the 43 years. Decadal variability in the MLD is also imprinted in the potential temperature profile in March. The vertical temperature profile versus time diagram (Figure 2c) indicates the presence of convection that homogenizes the water column from the surface to variable depths, depending upon the convective intensity. Colder water in the region suggests deeper penetration, and warmer temperatures suggest convection to shallower depths. Distinctively strong mixing events occur from 1971 to 1972 and from 1983 to 1984, reaching depths of roughly 2000 m. The temperature varies from 1.9°C to 4.4°C and fluctuates at decadal timescales with an amplitude of approximately 0.7°C . The event in the early 1960s is also considered as a strong event although it does not appear as strong. This may be related to the fact that the decadal oscillation is embedded in the long-term trend in the temperature field. In the numerical simulation, the long-term trend is induced from the model drift and therefore it is impossible to discern the model drift and the natural long-term trend in

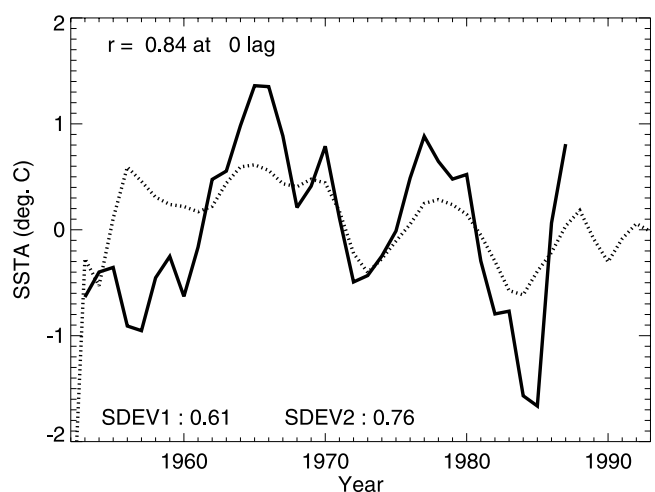


Figure 3. Sea surface temperature anomalies (SSTA) binomial-filtered once and linearly detrended. The dotted line is the SSTA in March obtained from the coupled ice-ocean model, averaged over the region shown in Figure 1d. The solid line is the observed SSTA time series from 1953 through 1987 from Houghton [1996]. Both time series from 1960 to 1987 are highly correlated with each other ($r = 0.84$ at 0 lag). $SDEV1$ and $SDEV2$ are the standard deviations for the dotted and solid lines, respectively.

this study. However, our focus is on the decadal oscillation that occurs roughly every 10 years in the LS.

[20] The time series of sea surface temperature anomalies (SSTA) from the coupled ice-ocean model in March, which is averaged over the region shown in Figure 1d, is highly correlated to that from the SSTA in March in observational analysis by *Houghton* [1996] (Figure 3) in particular after 1960 ($r = 0.84$ at 0 lag). The period of oscillation is nearly identical in both time series.

3.2. Region of Deep-Water Formation

[21] The region of deep-water formation (Figure 1d) coincides with that estimated from observations. A salinity map [*Lilly et al.*, 1999, Figure 2] on the $\sigma_0 = 27.72 \text{ kg/m}^3$ isopycnal during 1965–1967 shows the region where the deep convection took place. The central salinity minimum, which was trapped by the cyclonic currents and considered to be a center of convection, was located at about 51.5°W , 57°N . The second salinity minimum that was identified as 34.88 psu extended roughly from 49°W to 56°W , 54°N to 59°N . The low-salinity extension of the LSW flowed southeastward along the continental slope out of the LS domain [*Pickart et al.*, 1997]. Other observational evidence of the convection site in the LS is presented by *Gascard and Clarke* [1983] and *Pickart et al.* [2002]. The geographical reason that the region of deep-water formation is located adjacent to the eastern Labrador coast seems to be related to the fact that wintertime cold and dry wind is needed to make the surface water dense enough to sink into the deeper water. These preferred atmospheric characteristics are typically found over the open ocean just near the land or ice boundaries. It is expected that the strength of the heat flux or the surface buoyancy flux (surface conditions) controls the intensity of the convection. The cyclonic ocean circulation dynamically creates the doming effect of the isopycnals toward its center (preconditioning). This effect sets up the condition for the weakly stratified underlying water to easily ventilate to the surface during the wintertime cooling and mixing. The intensity of the convective activity seems to be attributed either to the oceanic surface conditions or the oceanic interior structure in the preconditioning stage, prior to a convection. The two major different roles will be described in more detail in the following subsection.

3.2.1. Surface Conditions

[22] The coupled ice-ocean model calculates the heat and salinity fluxes using the oceanic surface conditions. The surface buoyancy flux is computed from the heat and salinity fluxes, and is integrated over the period from November to March to yield the time integrated surface buoyancy flux (B) (Figure 4a). This is the time when the violent mixing resumes until the maximum depth is reached over the course of a convection process. Values of B vary from year to year roughly ranging from $0.5 \text{ m}^2 \text{ s}^{-2}$ to $2.0 \text{ m}^2 \text{ s}^{-2}$, which correspond to the time-integrated surface buoyancy flux for about 1.5 to 6.0 months using a typical buoyancy flux value of $1.2 \times 10^{-7} \text{ m}^2 \text{ s}^{-3}$ in the LS [*Marshall and Schott*, 1999]. The time series of the MLD in March (Figure 2c) is correlated with that of surface buoyancy (Figure 4a) as $r = 0.45$ at 0 lag at the longer timescales. According to the model result it is suggested that the surface buoyancy over the deep-water formation region is not the only factor for determining the

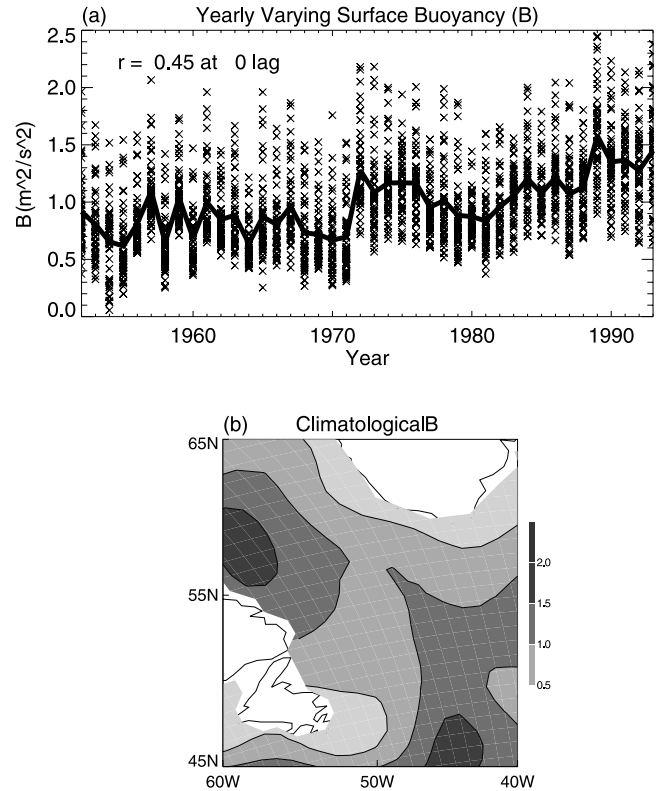


Figure 4. (a) Modeled surface buoyancy (B) ($\text{m}^2 \text{ s}^{-2}$) (time-integrated surface buoyancy flux from November to March) in each year over the region of deep-water formation shown in Figure 1d. All the values (crosses) over this region at each year are plotted. Superimposed is the time series averaged over this region at each year. The cross-correlation coefficient of $r = 0.45$ at 0 lag is shown on the top left corner between the time series of MLD in March (Figure 2c) and that of surface buoyancy. Both time series are binomial-filtered once and linearly detrended. (b) Climatological surface buoyancy in the horizontal obtained by averaging the time series from 1952 through 1993. A spatial Hanning filter is applied three times to make the field smooth.

convective intensity at the decadal timescales. The spatial pattern of the climatological surface buoyancy in the horizontal does not indicate particularly strong buoyancy over the deep-water formation site with the larger values to the north and south. A similar spatial distribution to that of the surface buoyancy is also found in the total heat flux during a wintertime obtained from the ECMWF model [*Lilly et al.*, 1999, Figure 3]. A local maximum for heat loss from the ocean to the atmosphere is located around 60°W , 60°N , which corresponds to the maximum surface buoyancy in the model. Hence it does not seem that the surface buoyancy preselects a preferred region in the LS.

3.2.2. Preconditioning

[23] Observations have shown that the spatial scale of convective chimneys in the LS is roughly $O(100 \text{ km})$ whereas that of atmospheric buoyancy forcing is $O(500 \text{ km})$ [*Gascard and Clarke*, 1983]. A model study by *Wallace and Lazier* [1988] suggested that atmospheric cooling may not be the only factor for a deep convection to

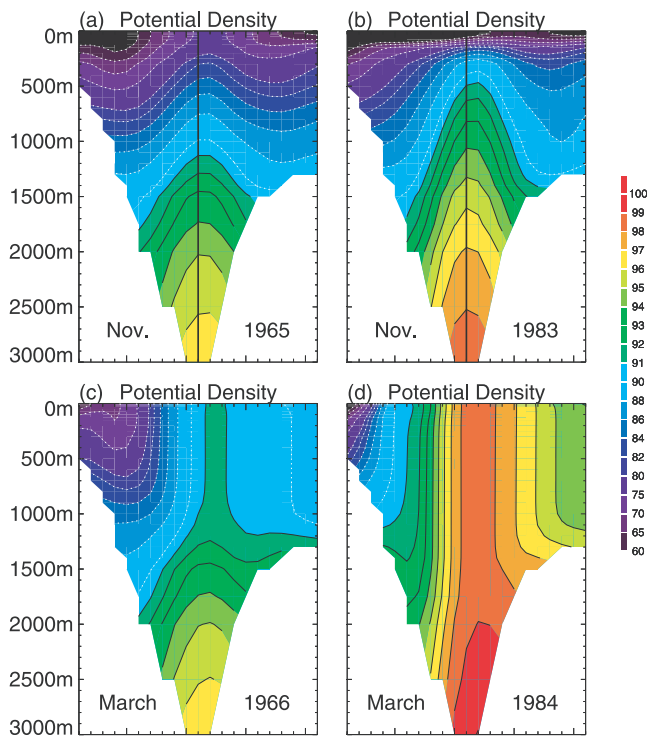


Figure 5. Vertical cross-section along the line (black circles) shown in Figure 1c in (a) precondition in November 1965, (b) precondition in November 1983, (c) violent mixing in March 1966, and (d) violent mixing in March 1984. It is viewed eastward from Newfoundland. The values are $(\sigma_\theta - 27.00) (\text{kg/m}^3) \times 100$. A spatial Hanning filter is applied three times to make the field smooth. Vertical density profiles along the black vertical lines in Figures 5a and 5b will be shown in Figure 7.

occur since most of the vertical profiles were not favorable for overturning below 1000 m under normal conditions. The deep convection could only be achieved with unrealistic heat fluxes. This implies that somehow the gyre-scale oceanic structure plays a key role for the selection of the convection site as well as the intensity of the penetration depth, and that the intensity of the convection is predetermined by the oceanic state at the preconditioning stage or determined by the combination of both the ongoing buoyancy forcing and the oceanic background stratification before the event occurs. In light of the oceanic “preconditioning” the domed isopycnals seem to significantly contribute to the selection of the convection site. The maximum density at the violent mixing stage in March (Figures 5c, 5d, 6c, and 6d) is always located at the center of the dome at the preconditioning stage in November (Figures 5a, 5b, 6a, 6b). Owing to the cyclonic gyre circulation the isopycnals are domed upward toward the center of the gyre. This effect creates a situation in which the isopycnals are lifted upward more toward the center, trapping the sharp vertical density gradient near the surface. The seasonal thermocline develops during summer-fall from the surface to approximately 200 m, and insulates the interior ocean from the surface conditions. In one sense, it places a lid at the surface, confining the relatively strong stratification just below 200 m. In order to convect deeply during the violent mixing

phase, significant cooling is first required to erode the seasonal thermocline and then further mixing takes place rather rapidly to the subsurface. *Straneo and Kawase* [1999] and *Alverson* [1995, chapter 4] demonstrated that the vertical structure of the domed isopycnals plays a key role in determining the depth of convective mixing. The magnitude of the vertical density gradient, from the near surface to the subsurface ocean, determines the depth of convection.

[24] Conditions before and after convection for 1965–1966 and 1983–1984 along the black circles in Figure 1c are shown to illustrate weak and strong periods of convection as seen in Figure 2c. We define that the oceanic state in November represents a precondition for convection that occurs in March in the following year. In November, 1983, isopycnals (Figure 5b) sharply dome upward toward the center of the cyclonic gyre, which further induces relatively strong stratification near the surface. In November 1965, the doming effect of the isopycnals (Figure 5a) appears much weaker compared to that in November 1983. The isopycnal 27.91 kg/m^3 , for example, increases its height about 700 m upward relative to its depth in November 1965 (Figure 5a). A maximum density of 27.98 kg/m^3 (Figure 5b) appears near the bottom in 1983 while its counterpart in November 1965 (Figure 5a) is 27.96 kg/m^3 , which also indicates the lifting of the isopycnals. In March 1984 (Figure 5d), chimneys are established due to the convective mixing, and all the isopycnals are vertically aligned. The mixed layer reaches a depth greater than 2000 m in 1983 (Figure 5d), whereas it only reaches a depth of 1000 m in March 1966 (Figure 5c). The vertical cross-section of the potential density, orthogonal to the above case (red circles in Figure 1c), demonstrates

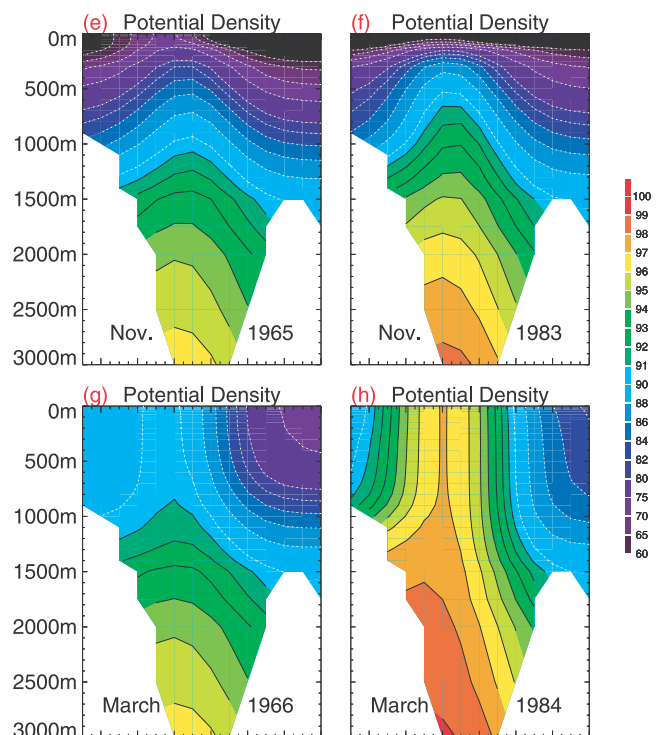


Figure 6. Same as Figure 5, except that the vertical cross-sections are now shown along the line of the red circles, which is orthogonal to the line of the black circles, shown in Figure 1c. It is viewed northward from the Atlantic ocean.

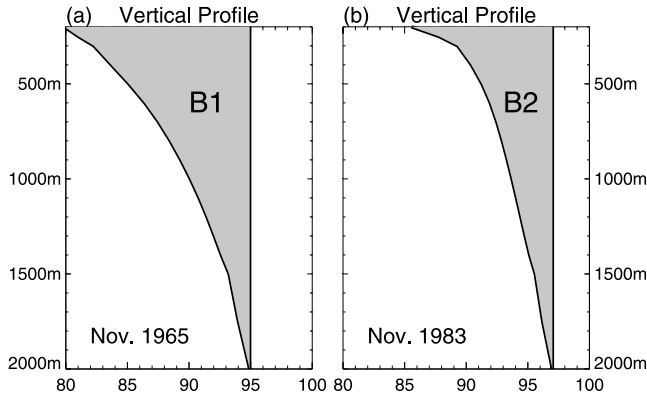


Figure 7. Vertical density profile in (a) November 1965 and (b) November 1983 along the vertical black line in Figures 5a and 5b, respectively. The depth extends from 200 m, just below the seasonal thermocline, to 2000 m. The x -axis ranges from 80 to 100 of the values defined as $(\sigma_\theta - 27.00) (\text{kg/m}^3) \times 100$. The shaded areas $B1$ and $B2$ are closed by the vertical density profile in November and vertically homogenized water column in March. Apparently in this case $B1 > B2$.

similarly the stronger doming effect of the isopycnals in November 1983 (Figure 6f) relative to that in November 1965 (Figure 6e). When the doming is stronger at the preconditioning stage the convection in March seems to result in more intense and deeper vertical mixing (Figure 6h). This also seems to be the reason why the two events in 1973 and 1983 both have deep convection although they are preceded by different surface conditions (Figures 1a and 1b). Regardless of the surface conditions, the intensity of the convective mixing depends upon the doming effect that is associated with the subsurface stratification in the preconditioning. In fact, the doming in November 1972 (not shown) is as strong as that in November 1982.

[25] A schematic figure from *Alverson* [1995, Figure 4.4b] provides a simple dynamical explanation for a link between the vertical density gradient and the convective depth. In November 1965 (Figure 7a), the density increases vertically from 27.80 kg/m^3 at 200 m to 27.95 kg/m^3 at 2000 m, whereas in November 1983 it increases from 27.86 kg/m^3 to 27.97 kg/m^3 . The vertical lines indicate the vertical density profiles in March if the water were to be mixed down to the depth of 2000 m. The sharp density gradient near the surface seen in Figure 5b acts to reduce the area ($B2$) while the dull density gradient near the surface seen in Figure 5a acts to widen the area ($B1$). If we consider the shaded area as the total buoyancy input at the ocean surface, or proportional to it, the relationship between the ocean surface condition and the subsurface precondition may be well established. When the isopycnals near the surface are sharply domed in the preconditioned ocean, compared to the weakly domed case, it is expected that less surface buoyancy is required in order to convect to the same depth. Conversely, with the same amount of buoyancy, the deeper mixing is expected in the case of the sharply domed isopycnals near the surface.

[26] Although the convective process is a complicated system in reality, we approximate the MLD in March

simply as a function of the total surface buoyancy flux integrated from November to March and the vertical density profile in November. In order to quantify the relationship, we apply a simple one-dimensional mixed-layer model used by *Alverson* [1995, equation (4.3)] in the following subsection. Our simple model refines the work of *Alverson* [1995] by including a yearly varying surface buoyancy flux.

3.3. One-Dimensional Mixed-Layer Model

[27] The MLD in March is diagnosed using the time-integrated surface buoyancy flux and the ocean vertical density profile at the preconditioning stage in November, just before convection occurs. This calculation involves only the vertical (z) dynamics. The MLD in March is chosen to represent the greatest depth of convection during the year. The density profile in November is selected as the preconditioning state because in some years the convective events resume in December. For convenience, the November before the convection is considered as the initial condition for the following year. For example, the precondition in November 1951 is labeled as 1952. This diagnostic calculation is performed each year from 1952 through 1993.

[28] An analytical one-dimensional mixed-layer model (equation (1)), that assumes only vertical dynamics, is used to estimate the depth of convection during the violent mixing stage at an arbitrary location and year.

[29] This model is calculated by

$$B = \frac{g}{\rho_0} \int_0^d (\rho(d) - \rho(z)) dz, \quad (1)$$

where $d = d(z)$ is a MLD to be estimated from the above equation, B is the time-integrated surface buoyancy flux, g is the gravity, ρ_0 is the mean density, $\rho(z)$ is the initial background stratification in November, and $\rho(d)$ is the uniform density profile mixed to the depth d in March. The equation is numerically integrated to a depth d , at which the given equation holds.

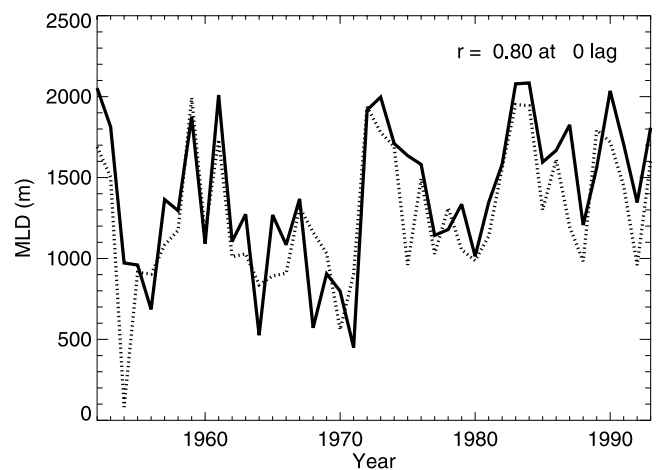


Figure 8. Time series of obtained MLD (dotted line) in March from the coupled ice-ocean model output and estimated MLD (solid line) in March, diagnosed using an analytical one-dimensional mixed-layer model (equation (1)). Both time series are averaged over the region shown in Figure 1d. They are highly correlated with each other with the cross-correlation coefficient of $r = 0.80$ at 0 lag.

[30] The estimated MLD (d) is averaged over the region of deep-water formation (Figure 1d). The time series contains both the high frequencies at the interannual timescales and the low frequencies at the decadal timescales. The time series of MLD estimated from the mixed-layer model (estimated MLD) and that of MLD directly obtained from the coupled ice-ocean model (obtained MLD) are highly correlated ($r = 0.80$ at 0 lag) and have similar amplitudes (Figure 8). This suggests that the one-dimensional mixed-layer model is capable of reproducing most of the variability in the convective activity in the LS shown by the coupled ice-ocean model. It is also suggested that not only the surface forcing but also the oceanic internal structure plays an important role in determining the depth of convection, according to the coupled ice-ocean model results.

3.4. Surface Buoyancy Versus Preconditioning at the Decadal Timescales

[31] The obtained and estimated MLD from the above calculation are highly correlated at the decadal timescales. When they are linearly detrended and binomial-filtered once

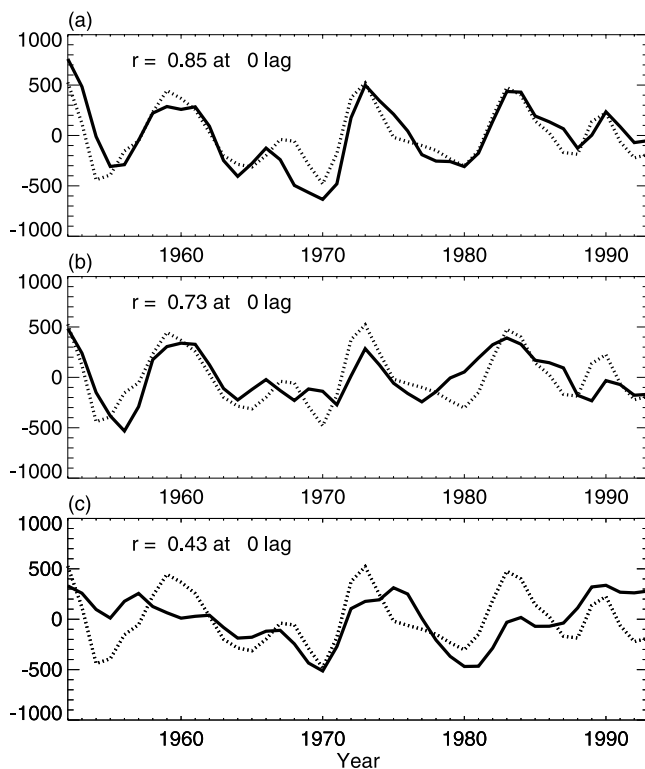


Figure 9. Time series of obtained MLD (dotted line) in March from the coupled ice-ocean model output and estimated MLD (solid line) in March, diagnosed using an analytical one-dimensional mixed-layer model (equation (1)): (a) same as Figure 8, (b) forced with realistic ocean stratification in November (as in Figures 5a–5b and 6a–b) and the climatological buoyancy (as in Figure 4b), and (c) forced with climatological ocean and realistic buoyancy. Both time series are averaged over the region shown in Figure 1d. All of the time series are linear-detrended and binomial-filtered once. The cross-correlation coefficients at 0 lag are shown on the top left corner.

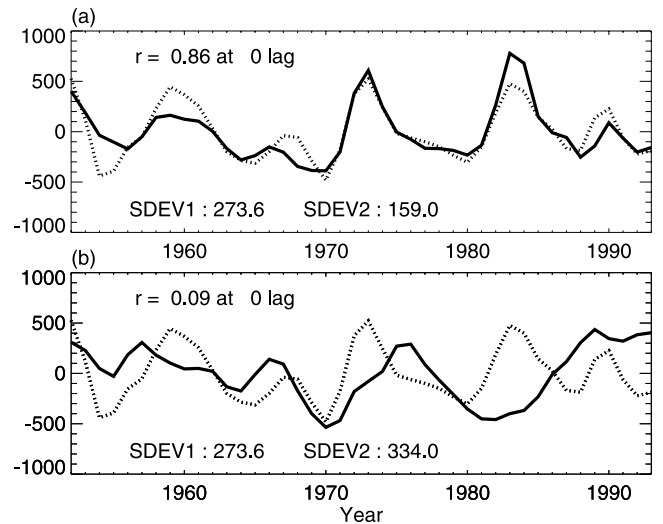


Figure 10. Same as Figure 8 except (a) the time series of estimated MLD (solid line) whose oceanic stratification in November is constructed with the realistic temperature and the climatological salinity and (b) with realistic salinity and the climatological temperature. $SDEV1$ is the standard deviation of the obtained MLD and $SDEV2$ of the estimated MLD. Note that the time series of estimated MLD is multiplied by ($SDEV1/SDEV2$) to make the amplitudes of the two time series comparable.

in order to extract the decadal signal, the correlation between the two time series is increased from $r = 0.80$ to 0.85 (Figure 9a). Since the one-dimensional mixed-layer model consists of the time-integrated surface buoyancy and the oceanic stratification at the preconditioning, the relative contribution of the two components to determining the MLD can be investigated by two experiments, in which either one of the components is kept constant with respect to time. The analytical model is calculated with the yearly varying oceanic stratification in November and the climatological buoyancy, which is averaged over the deep-water formation region and plotted from 1952 to 1993 (Figure 9b). Both the time series of the obtained and estimated MLD are detrended and binomial-filtered once. They are highly correlated with each other ($r = 0.73$ at 0 lag). This suggests that the decadal variability of the MLD is highly correlated to the variability of the subsurface oceanic stratification at the preconditioning stage. In the case with the yearly varying buoyancy and the climatological oceanic stratification (Figure 9c), the estimated MLD does not correlate with the obtained MLD ($r = 0.43$ at 0 lag), indicating that the role of buoyancy forcing alone cannot explain the decadal variability in the region of interest. The important role of oceanic stratification in the precondition for convection seems clear for the decadal timescales.

[32] The contribution of temperature and salinity to the density is shown by reconstructing the density with the yearly varying temperature and the climatological salinity in November (Figure 10a) and with the yearly varying salinity and the climatological temperature in November (Figure 10b). The buoyancy obtained from the coupled ice-ocean model is included in the calculation. This run is

basically the same as Figure 9 except that the oceanic stratification has only either the temperature or salinity component. The time series with the former component, i.e., Figure 10a, has a similar amplitude as the obtained MLD and is highly correlated to it ($r = 0.86$ at 0 lag). On the other hand, the salinity contribution to the stratification is almost zero in case of Figure 10b. Thus the variability of the subsurface stratification is associated with the subsurface temperature changes.

4. Summary and Discussion

[33] A 43-year subset of output from a coupled ice-ocean model has been analyzed to study the decadal variability in the Labrador Sea (LS). The high surface densities or the deepest mixed layer in March, indicating the convective region, are located in the interior on the western part of the Labrador basin. Evidence of the decadal variability in the convective activity is seen in the temperature versus time diagram. Every year the mixing reaches a depth of at least 1000 m. Distinctively strong convective events occur from 1971 to 1972 and from 1983 to 1984, reaching depths greater than 2000 m. The modeled data reproduce the frequency of the convective events that are seen in the observations [Lazier, 1980; Dickson *et al.*, 1996; Curry *et al.*, 1998; Dickson *et al.*, 2002] relatively well at the decadal timescales.

[34] The cyclonic circulation in the LS sets up a favorable condition for deep convection, where the domed isopycnals play a role of oceanic preconditioning. The precondition in November significantly contributes to not only the determination of the convection site but also the convection depth. Sharply domed isopycnals near the surface increase the vertical density gradient there.

[35] An analytical one-dimensional mixed-layer model is used to diagnose the mixed layer depth (MLD) in March from the oceanic density profile in November and the external buoyancy forcing, and compare with the MLD directly obtained from the output of the coupled ice-ocean model in March. The one-dimensional mixed-layer model reproduces most of the variability, which is derived from the coupled ice-ocean model, in the convective depth in the LS at the decadal timescales ($r = 0.85$ at 0 lag). With a yearly varying oceanic density profile in November and the climatological buoyancy the model produces the decadal fluctuation considerably well ($r = 0.73$ at 0 lag). The decadal variability of the MLD is highly correlated to that of the subsurface ocean stratification at the preconditioning stage. The surface buoyancy forcing alone does not completely explain the decadal processes in the region of interest. Furthermore, the oceanic density profile, calculated from the yearly changing temperature and climatological salinity, has variability very similar to that of the model density, suggesting that the variability of the vertical stratification is associated with temperature changes in the subsurface ocean.

[36] In this study, the causes of the decadal variations in the convective mixing have not been discussed. Houghton and Visbeck [2002] attributed the quasi-decadal fluctuations in the LS to local processes. They found that variations of the windstress and therefore the local heat flux over the LS controls the variation of the convective mixing. The oceanic

stratification acts simply to modulate the convective depth, which is primarily determined by the magnitude of the heat flux over the LS. According to our model, the oceanic stratification rather controls the variations of the convective depth to large extent at the decadal timescales. With a given heat flux the convective depth can vary considerably, depending upon how strong the isopycnal doming is in the preconditioning.

[37] In contrast to the local scenario of Houghton and Visbeck [2002], we look to the North Atlantic outside of the LS for the source of the quasi-decadal fluctuations. An observational study by Reverdin and Verbrugge [1999] showed that 50% of the heat content changes in the subpolar gyre can be explained by the local heat flux from 1993 through 1998 while the rest is transported to the LS from outside of the subpolar gyre. We speculate that the decadal changes in the subsurface stratification or the doming effect are associated with the changes in the upper heat content and further that the upper ocean heat content changes are brought into this region from the outside of the LS. Häkkinen [2000] demonstrated that the upper 1000-m heat content anomalies propagate from the eastern boundary in the midlatitude in the form of decadal Rossby waves and advect northward into the subpolar region along the western boundary. She proposed the active involvement of the thermohaline circulation (THC) via the changes in the convective activity in the LS. The decadal Rossby waves are considered as a delayed response to the changes in the THC. The northward propagating anomalies along the western boundary were first recognized by Sutton and Allen [1997], who analyzed the observed SSTA along the western boundary region. Because of their slow speed ($\sim 1.7 \text{ cm s}^{-1}$), they speculated that the SST signals represent the upper ocean transport below the mixed layer. Other observational data indicated that the decadal signals exist in the subsurface in the western boundary current [Molinari *et al.*, 1997]. The observations support the propagating nature of the upper heat transport along the Gulf Stream.

[38] Of course, the roles of the heat flux and lateral eddy flux in the local processes or perhaps other external factors such as fresh water import to the LS are not dismissed as the causes. Local heat flux from previous years could be accumulated in the LS and the lateral eddy flux would participate in the restratification process to shape up the isopycnal doming. However, the remote scenario presented here could potentially explain the dynamical link to the variations in the LS found in the model, as also suggested by the observational study of Reverdin and Verbrugge [1999].

[39] Further investigation on the connection between the basin-wide oscillation and the convective activity in the LS will help explain the decadal mechanism found in the North Atlantic. Modeling work will be one of the options to examine the propagating nature of the basin-wide oscillation.

[40] In the present study, we have shown that the combined effects needed to set up the preconditioning associated with the subsurface stratification, rather than solely the local heat flux, determines the intensity of the convective mixing. Even though nature consists of a very complicated system, we believe that the model sufficiently extracts the decadal variation that potentially exists as one

component among many other natural modes of the decadal variability in the ocean.

[41] **Acknowledgments.** This work was supported by the National Oceanic and Atmospheric Administration grant NA76GP0521, National Aeronautics and Space Administration grant NAG5-8327, and the Office of Naval Research, Secretary of the Navy grant N00014-94-1-0369, which provides the base support for the research conducted by James J. O'Brien, Director, Center for Ocean-Atmospheric Prediction Studies, at Florida State University. The coupled ice-ocean model output was produced at NASA Goddard Space Flight Center. The authors wish to thank Thierry Penduff for helpful discussions and suggestions. We sincerely thank the two anonymous reviewers who gave valuable comments and suggestions to clarify the text and Denise L. Worthen for help in the preparation of this text.

References

- Alverson, K. D., Topographic preconditioning of open-ocean deep convection, Ph.D. dissertation, 146 pp., Mass. Inst. of Technol., Cambridge, Mass., 1995.
- Belkin, I. M., S. Levitus, J. Antonov, and S. A. Malmberg, "Great Salinity Anomalies" in the North Atlantic, *Prog. Oceanogr.*, **41**, 1–68, 1998.
- Blumberg, A. F., and G. L. Mellor, A description of a three-dimensional coastal ocean circulation model, in *Three-Dimensional Coastal Ocean Models*, *Coastal Estuarine Stud.*, vol. 4, edited by N. S. Heaps, pp. 1–16, AGU, Washington, D. C., 1987.
- Curry, R. G., M. S. McCartney, and T. M. Joyce, Oceanic transport of subpolar climate signals to mid-depth subtropical waters, *Nature*, **391**, 575–577, 1998.
- Deser, C., and M. L. Blackmon, Surface climate variations over the North Atlantic Ocean during winter: 1900–1989, *J. Clim.*, **6**, 1743–1753, 1993.
- Dickson, B., I. Yashayaev, J. Meincke, B. Turrell, S. Dye, and J. Holfort, Rapid freshening of the deep North Atlantic Ocean over the past four decades, *Nature*, **416**, 832–837, 2002.
- Dickson, R. R., J. Meincke, S.-A. Malmberg, and A. J. Lee, The "Great Salinity Anomaly" in the Northern North Atlantic 1968–1982, *Prog. Oceanogr.*, **20**, 103–151, 1988.
- Dickson, R. R., J. Lazier, J. Meincke, P. Rhines, and J. Swift, Long-term coordinated changes in the convective activity of the North Atlantic, *Prog. Oceanogr.*, **38**, 241–295, 1996.
- Drinkwater, K. F., Climate and Oceanographic variability in the Northwest Atlantic during the 1980s and early 1990s, *SCR Doc. 94/71*, pp. 1–39, Northwest Atlantic Fish. Org., Dartmouth, N. S., Canada, 1994.
- Gascard, J. C., and R. A. Clarke, The formation of Labrador Sea water: II. Mesoscale and smaller-scale processes, *J. Phys. Oceanogr.*, **13**, 1779–1797, 1983.
- Häkkinen, S., Variability of the simulated meridional heat transport in the North Atlantic for the period 1951–1993, *J. Geophys. Res.*, **104**(C5), 10,991–11,007, 1999.
- Häkkinen, S., Decadal air-sea interaction in the North Atlantic based on observations and modeling results, *J. Clim.*, **13**, 1195–1219, 2000.
- Häkkinen, S., and G. L. Mellor, Modeling the seasonal variability of the coupled arctic ice-ocean system, *J. Geophys. Res.*, **97**(C12), 20,285–20,304, 1992.
- Holland, M. M., C. M. Bitz, M. Eby, and A. J. Weaver, The role of ice-ocean interactions in the variability of the North Atlantic thermohaline circulation, *J. Clim.*, **14**, 656–675, 2001.
- Houghton, R. W., Surface Quasi-Decadal Fluctuations in the North Atlantic, *J. Clim.*, **9**, 1363–1373, 1996.
- Houghton, R. W., and M. H. Visbeck, Quasi-decadal Salinity Fluctuations in the Labrador Sea, *J. Phys. Oceanogr.*, **32**, 687–701, 2002.
- Killworth, P. D., The mixing and spreading phases of MEDOC: I, *Prog. Oceanogr.*, **7**, 59–90, 1976.
- Klinger, B., J. Marshall, and U. Send, Representation of convective plumes by vertical adjustment, *J. Geophys. Res.*, **101**(C8), 18,175–18,182, 1996.
- LabSeaGroup, The Labrador Sea Deep Convection Experiment, *Bull. Am. Meteorol. Soc.*, **79**(10), 2033–2058, 1998.
- Lazier, J. R. N., Oceanographic conditions at Ocean Weather Ship Bravo, 1964–1986, *Atmos. Ocean*, **18**, 227–238, 1980.
- Lilly, J. M., P. B. Rhines, M. Visbeck, R. Davis, J. R. N. Lazier, F. Schott, and D. Farmer, Observing deep convection in the Labrador Sea during winter 1994/95, *J. Phys. Oceanogr.*, **29**, 2065–2098, 1999.
- Marshall, J., and F. Schott, Open ocean convection: Observations, theory, and models, *Rev. Geophys.*, **37**(1), 1–64, 1999.
- Mauritzen, C., and S. Häkkinen, Influence of sea ice on the thermohaline circulation in the Arctic-North Atlantic Ocean, *Geophys. Res. Lett.*, **24**, 3257–3260, 1997.
- Mellor, G. L., and T. Yamada, Development of a turbulence closure model for geophysical fluid problems, *Rev. Geophys.*, **20**, 851–875, 1982.
- Mizoguchi, K., S. D. Meyers, S. Basu, and J. J. O'Brien, Multi- and quasi-decadal variations of sea surface temperature in the North Atlantic, *J. Phys. Oceanogr.*, **29**, 3133–3144, 1999.
- Molinari, R. L., D. A. Mayer, J. F. Festa, and H. F. Bezdek, Multiyear variability in the near-surface temperature structure of the midlatitude western North Atlantic Ocean, *J. Geophys. Res.*, **102**(C2), 3267–3278, 1997.
- Pickart, R. S., M. A. Spall, and J. R. N. Lazier, Mid-depth ventilation in the western boundary current system of the sub-polar gyre, *Deep Sea Res.*, **44**(6), 1025–1054, 1997.
- Pickart, R. S., D. J. Torres, and R. A. Clarke, Hydrography of the Labrador Sea during active convection, *J. Phys. Oceanogr.*, **32**, 428–457, 2002.
- Rasmusson, E. M., and K. Mo, Large scale atmospheric moisture cycling as evaluated from NMC global analysis and forecast products, *J. Clim.*, **9**, 3276–3297, 1996.
- Reverdin, G., and N. Verbrugge, Upper ocean variability between Iceland and Newfoundland, *J. Geophys. Res.*, **104**(C12), 29,599–29,611, 1999.
- Reverdin, G., D. Cayan, and Y. Kushnir, Decadal variability of hydrography in the upper northern North Atlantic in 1948–1990, *J. Geophys. Res.*, **102**(C4), 8505–8531, 1997.
- Send, U., and J. Marshall, Integral effects of deep convection, *J. Phys. Oceanogr.*, **25**, 855–872, 1995.
- Straneo, F., and M. Kawase, Comparison of localized convection due to localized forcing and to preconditioning, *J. Phys. Oceanogr.*, **29**, 55–68, 1999.
- Sutton, R. T., and M. R. Allen, Decadal predictability of North Atlantic sea surface temperature and climate, *Nature*, **388**, 563–567, 1997.
- United Nations Educational, Scientific and Cultural Organization, Tenth report of the joint panel on oceanographic tables and standards, *UNESCO Tech. Pap. Mar. Sci.*, **36**, Paris, 1981.
- Visbeck, M., J. Marshall, and H. Jones, Dynamics of isolated convective regions in the ocean, *J. Phys. Oceanogr.*, **26**, 1721–1734, 1996.
- Wallace, D. W. R., and J. R. N. Lazier, Anthropogenic chlorofluoromethanes in newly formed Labrador Sea Water, *Nature*, **332**, 61–63, 1988.
- S. Häkkinen, NASA Goddard Space Flight Center, Code 971, B33, Room A221, Greenbelt, MD 20771, USA. (sirpa@ltpmail.gsfc.nasa.gov)
- K. Mizoguchi, Goddard Earth Sciences and Technology (GEST), University of Maryland at Baltimore County, 1000 Hilltop Circle, Baltimore, MD 21250, USA. (mizoguchi@ltpmailx.gsfc.nasa.gov)
- S. L. Morey, J. O'Brien, and J. Zavala-Hidalgo, Suite 200, Johnson Building, 2035 East Paul Dirac Drive, Tallahassee, FL 32310, USA. (morey@coaps.fsu.edu; obrien@coaps.fsu.edu; zavala@coaps.fsu.edu)
- N. Sugimotohara, Frontier Observational Research System for Global Change, 3173-25 Showa-machi, Kanazawa-ku, Yokohama Kanagawa, 237-0001, Japan. (nobuo@jamstec.go.jp)